NuMI-112
PDK-626
Nov. 10, 1995

Neutrino Cross Sections

H. M. Gallagher and M. C. Goodman

Nov. 10, 1995

Abstract

The Fermilab wide band neutrino beam spectrum spans an energy range where a number of neutrino scattering mechanisms are important. In this paper we will present neutrino cross sections separately for 3 processes: quasi-elastic, resonance production, and deep inelastic scattering. We will attempt to extend the calculations where necessary to incorporate ν_τ interactions. We will then discuss the construction of σ_{tot} from the above three processes. Throughout, we will attempt to describe the uncertainties in these cross-sections, appealing to data wherever possible to check the overall accuracy and consistency of our predictions. In particular, this work will describe the cross-sections used in the Soudan 2 Monte Carlo.

1 Introduction

The Fermilab Main Injector wide band beam offers a unique opportunity to do neutrino physics in the energy range from 1 to 100 GeV. For a typical Main Injector flux spectrum with mean energy $\langle E_\nu \rangle \approx 13$ GeV, and incorporating the cross-sections which will be described in this document, 5% of charged current neutrino interactions are quasi-elastic, 13% are resonance production, and 82% are deep inelastic scattering. This 'medium' energy range is somewhat problematic because it lies at the transition region between our two intuitive models for neutrino interactions. At low energies, which are well understood phenomenologically, neutrino scatterings are predominantly quasi-elastic, in which the target is taken to be an entire nucleon. At high energies, neutrino interactions are mainly deep inelastic scattering, where the target is one of the constituent partons inside the nucleon. Again in this region the theoretical and experimental situations are well in hand. In the medium energy ($\approx$ 10 GeV) range, the concept of a well-defined 'target' is more tenuous, as both quasi-elastic and DIS interactions can occur. This uncertainty can be viewed as a consequence of the fact that we are pushing the limits of perturbative QCD, and the assumptions underlying the derivation of DIS formulae are less valid. These theoretical difficulties are particularly evident in the lack of a uniform treatment of neutrino resonance production. The decay of these resonance states feeds into the low multiplicity channels. Hadronic final states consisting of a nucleon and a single pion are primarily the result of the decay of a low mass resonance (such as the $\Delta(1232)$). A related problem is determining the total charged current cross section in this medium energy range in terms of these 3 processes. Fortunately,

data exists in this energy range and can be used to check both the overall normalization, σ_{tot}, and the relative contribution of low multiplicity channels.

An additional cross-section issue that needs to be dealt with for a neutrino oscillation search is calculating ν_τ cross sections. Terms proportional to lepton mass $(m_l/M)^2$ are negligible in ν_μ or ν_e interactions and are typically ignored. Form factors which are unmeasured in neutrino experiments with electron and muon neutrinos (because they appear in terms proportional to $(m_l/M)^2$) can become important for ν_τ interactions. Parametrizations for these form factors must thus be taken on purely theoretical grounds.

More details on the Soudan 2 Monte Carlo neutrino event generator of specific interest to atmospheric neutrino studies can be found in Reference [1].

2 Quasi-Elastic Scattering

At low neutrino energies, charged current neutrino-hadron interactions are predominantly quasi-elastic and single pion production, in which the neutrino scatters off an entire nucleon rather than the constituent partons. These processes have been studied with in low energy (100 MeV - 10 GeV) bubble chamber experiments. The general hadronic current can be decomposed in terms of its Lorentz structure as [2]

$$< P(p') \mid J_\mu^- \mid N(p) >= \tag{1}$$

$$\overline{P}(p')\Big[F_V^1\gamma_\mu + \frac{i\sigma_{\mu\nu}q^\nu\xi F_V^2}{2M} + \frac{q_\mu F_S}{M} + F_A\gamma_5\gamma_\mu + \frac{F_P\gamma_5 q_\mu}{M} + \frac{\gamma_5(p+p')_\mu F_T}{M}\Big]N(p)$$

where F_S, F_P, F_V, F_A, F_T describe the scalar, pseudoscalar, vector, axial-vector, and tensor form factors of the nucleon, respectively. $q = (p - p')$, where p is the 4-momentum of the target nucleon and p' is the 4-momentum of the outgoing nucleon.

The differential cross section for the quasi-elastic process can be written in the lab frame of reference, where the neutrino has energy E_ν, the target nucleon of mass M is at rest, and the Mandelstam invariants are s, $t = q^2$, and u [2]:

$$\frac{d\sigma}{d|q^2|}\begin{pmatrix}\nu n \to l^- p\\ \overline{\nu} p \to l^+ n\end{pmatrix} = \frac{M^2G^2cos^2\theta_c}{8\pi E_\nu^2}\Big[A(q^2) \mp B(q^2)\frac{(s-u)}{M^2} + \frac{C(q^2)(s-u)^2}{M^4}\Big]. \tag{2}$$

In this expression, G is the Fermi coupling constant and θ_c is the Cabibbo mixing angle ($G = 1.16639 \times 10^{-5}\mathrm{GeV}^{-2}$). The functions A, B, and C are convenient combinations of the nucleon form factors.

Contraction of the hadronic and leptonic currents yields:

$$A = \frac{(m^2-q^2)}{4M^2}\Big[\Big(4-\frac{q^2}{M^2}\Big)|F_A|^2 - \Big(4+\frac{q^2}{M^2}\Big)|F_V^1|^2 - \frac{q^2}{M^2}|\xi F_V^2|^2\Big(1+\frac{q^2}{4M^2}\Big) - \frac{4q^2 ReF_V^{1*}\xi F_V^2}{M^2} \tag{3}$$

$$+\frac{q^2}{M^2}\Big(4-\frac{q^2}{M^2}\Big)|F_T|^2 - \frac{m^2}{M^2}\Big(|F_V^1+\xi F_V^2|^2 + |F_A+2F_P|^2 + \Big(\frac{q^2}{M^2}-4\Big)\Big(|F_S|^2+|F_P|^2\Big)\Big)\Big]$$

$$B = -\frac{q^2}{M^2} Re F_A^* (F_V^1 + \xi F_V^2) - \frac{m^2}{M^2} Re\left[\left(F_V^1 + \frac{q^2}{4M^2}\xi F_V^2\right)^* F_S - \left(F_A + \frac{q^2 F_P}{2M^2}\right)^* F_T\right] \quad (4)$$

$$C = \frac{1}{4}\left(|F_A|^2 + |F_V^1|^2 - \frac{q^2}{M^2}\left|\frac{\xi F_V^2}{2}\right|^2 - \frac{q^2}{M^2}|F_T|^2\right), \quad (5)$$

where m is the final state lepton mass. Ignoring second-class currents (those which violate G-parity) allows us to set the scalar and tensor form factors to zero. According to the CVC hypothesis, the vector part of the weak current and the isovector part of the electromagnetic current form a isotriplet of conserved currents [3]. This hypothesis allows us to relate F_V^1 and F_V^2 to the electromagnetic form factors, which are better measured. In terms of the Sachs form factors,

$$F_V^1(q^2) = \left(1 - \frac{q^2}{4M^2}\right)^{-1} [G_E^V(q^2) - \frac{q^2}{4M^2} G_M^V(q^2)] \quad (6)$$

$$\xi F_V^2(q^2) = \left(1 - \frac{q^2}{4M^2}\right)^{-1} [G_M^V(q^2) - G_E^V(q^2)]. \quad (7)$$

The electromagnetic form factors are determined from electron scattering experiments:

$$G_E^V(1^2) = \frac{1}{(1 - \frac{q^2}{M_V^2})^2} \qquad G_M^V(q^2) = \frac{1 + \mu_p - \mu_n}{(1 - \frac{q^2}{M_V^2})^2}. \quad (8)$$

The situation is slightly more complicated for the hadronic axial current. $F_A(q^2 = 0) = -1.261 \pm .004$ is known from neutron beta decay. The q^2 dependence has to be inferred or measured. By analogy with the vector case we assume the same dipole form:

$$F_A(q^2) = \frac{-1.23}{(1 - \frac{q^2}{M_A^2})^2}. \quad (9)$$

The q^2 dependence of the differential scattering cross section has been measured in low energy experiments [6, 8], and agrees well with the above expression. Terms proportional to m_l, ignorable for ν_μ and ν_e interactions, are non-negligible for ν_τ interactions. Therefore some assumptions must be made about the pseudoscalar form factor F_p. One can use the PCAC hypothesis, $\partial_\mu j_A^\mu = m_\pi^3 f_\pi \phi_\pi(x)$ [4, 5] (where f_π is the pion decay constant and ϕ_π is the pion field), to postulate a form for F_P. A plausible parametrization that satisfies PCAC at low q^2 is [2]

$$F_P(q^2) = \frac{2M^2 F_A(q^2)}{M_\pi^2 - q^2}. \quad (10)$$

The inclusion of F_P leads to an approximately 5% reduction in both the ν_τ and $\overline{\nu}_\tau$ quasi-elastic cross sections. The only remaining parameters needed to describe the quasi-elastic cross section are thus M_V and M_A. $M_V = .71$ GeV, as determined with high accuracy

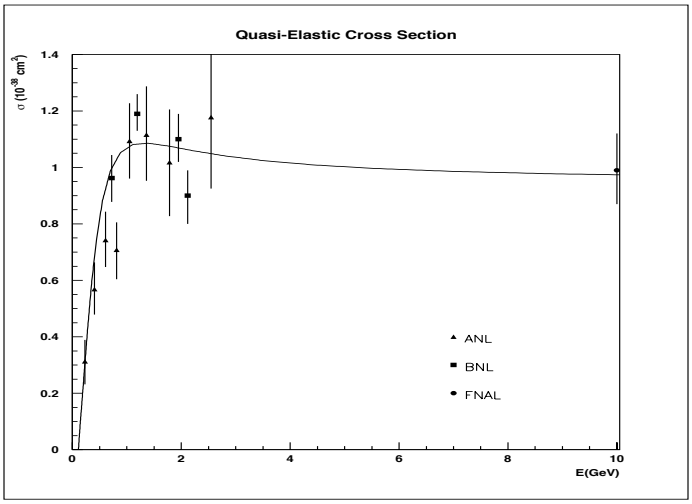

Figure 1: Quasi-Elastic Cross Sections

through electron scattering experiments [6]. M_A needs to be extracted from neutrino scattering data. From analyzing total cross sections and kinematic distributions for quasi-elastic neutrino-nucleon scattering, a global average value of the axial-vector mass is found to be $M_A = 1.032 \pm .036$ GeV [7]. The uncertainties on the axial-vector mass encompass the uncertainties for ν_μ charged current quasi-elastic scattering. The uncertainties on the ν_τ cross section are necessarily larger because of the complete lack of knowledge regarding the pseudo-scalar form factor.

The predicted quasi-elastic cross section as a function of energy is shown in Figure 1 as a solid line along with data from the Argonne 12' [8], BNL 7' [6], and FNAL 15' [9] bubble chamber experiments.

2.1 Nuclear Effects

In the previous discussion, we have treated the target nucleons as free bodies inside the target material. However, since the nucleons must be bound inside the nuclei, there may be many-body interactions (that necessarily depend upon the type of nucleus) which modify this naïve prediction. Of great concern is the fact that low energy measurements of quasi-elastic scattering have primarily been made on deuterium targets, while we are interested in these processes on heavier targets, primarily iron. Nuclear target effects will necessarily change both the q^2 distributions and total cross sections. One difference is that the struck nucleon will now have some initial Fermi momentum from its confinement the nuclear potential well. This momentum is typically ≈ 200 MeV/c for iron. A second consideration is Pauli blocking,

which is a consequence of the Pauli Exclusion Principle applied to the nucleus. Small energy transfers to bound nucleons are forbidden because low-lying energy levels are already filled by other nucleons. The net result is a suppression of the differential cross section at low q^2. Calculations of these effects are usually done with a Fermi gas model of the nucleus, wherein all energy levels up to the Fermi momentum P_f are considered to be filled, and momentum transfers which leave the final state nucleon within the Fermi sphere, i.e. with momentum $|p| < P_f$, are 'blocked'. This is equivalent to multiplying the differential cross section by a response factor [10]

$$R(q,\omega) = \frac{1}{\frac{4}{3}\pi p_F^3} \int \frac{d^3 p M_p^2}{E_N E_{N'}} \delta(E_N + \omega' - E_{N'}) \Theta(p_F - |\vec{p}|) \Theta(|\vec{p} + \vec{q}| - p_F) \tag{11}$$

which leads to an approximately 20% reduction in the quasi-elastic cross section at low energies. While nuclear effects are less important for deep inelastic scattering processes, they can produce substantial reductions in the differential cross section in particular regions of phase space. Nuclear shadowing effects have been measured and can produce as much as a 20% reduction in the deep inelastic scattering differential cross section at very low x_{Bj} ($x_{Bj} \approx 10^{-3}$) [11].

3 Resonance Production

The resonance production model used in the Soudan Monte Carlo is based on the work of Rein and Seghal, which employs the Feynman, Kislinger and Ravndal model of baryon resonances [12, 13]. This model describes resonances in terms of excited states of the 3-quark system bound by a relativistic harmonic oscillator potential

$$H = 3(p_a^2 + p_b^2 + p_c^2) + \frac{1}{36}\Omega^2[(u_a - u_b)^2 + (u_b - u_c)^2 + (u_c - u_a)^2]. \tag{12}$$

The FKR model has been successfully applied to low energy pion scattering data. The Hamiltonian is solved for the bound state wave functions, which are then associated with the observed resonances. The production matrix elements can then be calculated according to

$$T(\nu N \to l N^*) = \frac{G}{\sqrt{2}}[\overline{u}_l \gamma^\beta (1 - \gamma_5) u_\nu] < N^* | J_\beta^+(0) | N > \tag{13}$$

where

$$J_\beta^+ = V_\beta - A_\beta \tag{14}$$

and $|N>, |N_*>$ are the state vectors for the struck nucleon and produced resonance, respectively. The above expression for the transition amplitude is simply the contraction of the lepton and nucleon weak currents. In the implementation in the Soudan Monte Carlo, interference between neighboring resonances that can affect the total $N\pi$ amplitude is not taken into account; production amplitudes are added coherently. At low energies, single pion production is dominated by production of the $\Delta(1232)$, while at higher energies higher

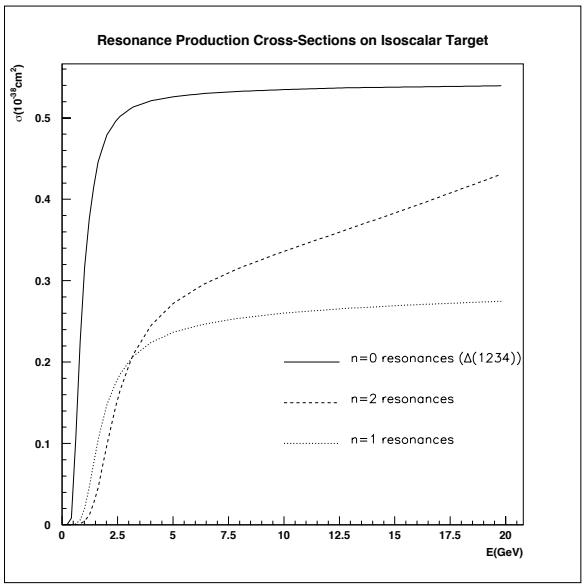

Figure 2: Resonance Production Cross Sections for differing n

mass resonances can also be produced. The energy dependence of the cross sections for various resonances is primarily a function of the principal oscillator quantum number, n, used to describe the 3-quark harmonic oscillator state. For n=0 states (the $\Delta(1232)$), the cross section saturates with energy at around 2 GeV, while n=1 states saturate at 10-20 GeV, and n=2 states exhibit a linear rise with energy. This is shown in Figure 2. This linear rise for the n=2 states is due to the dynamical structure of the FKR wavefunctions for n=2 oscillator states. There is also the additional complication that the region in phase space where the differential cross section increases dramatically at higher energies is kinematically disallowed for tau production. Hence n=2 resonances have a rising cross section for ν_μ and ν_e production but not for ν_τ, a discrepancy which is not reconcilable with the fact that, for $E_\nu \gg m_l$, the cross sections for these processes should approach the same value.

These predictions can be tested by comparing to data on single pion production in the $10 \sim 100$ GeV range. A comparison has been made to the invariant mass distribution for the process $\nu + p \rightarrow l + p + \pi^+$ from data taken by the BEBC collaboration [14]. This comparison has led us to conclude that the Rein and Seghal model, as it is incorporated in the Soudan Monte Carlo, overestimates the amount of resonance production at higher energies. This can be remedied in the Soudan Monte Carlo by limiting phase space integration for resonances to invariant masses less than some cutoff (perhaps 3 GeV). Data on single pion production from neutrinos and anti-neutrinos compiled by Reference [15] are compared to the predictions of the Soudan Monte Carlo model in Figures 3 and 4. In these figures, the isospin 1/2 channels

(plots B and C) in Figures 3 and 4 include contributions from deep inelastic scattering. The relative contribution of deep inelastic scattering to low multiplicity channels will be discussed in section 5.

Besides the Rein and Seghal model, which calculates transition amplitudes directly from the SU(6) quark wave functions, several other phenomenological descriptions of neutrino resonance production have been described in the literature. Methods involving calculations of dispersion relations, and isobar models in which the resonance is treated as an elementary particle have also been investigated by several authors [16, 17].

Note that the Rein and Seghal treatment of the hadronic current in Equation 14 ignores pseudoscalar terms, which we might expect to have an effect on the total cross sections for the resonance production by ν_τ's (as it does in quasi-elastic scattering). Because form factors which could produce additional reduction in the cross section have been neglected in the Rein and Seghal calculation, we have, by analogy with the quasi-elastic case, multiplied the total cross sections for tau production by an additional factor

$$g = \frac{\sigma(\nu_\tau n \to \tau^- p; F_A, F_V, F_P(PCAC))}{\sigma(\nu_\tau n \to \tau^- p; F_A, F_V, F_P = 0)} \tag{15}$$

for tau neutrino quasi-elastic scattering and

$$\overline{g} = \frac{\sigma(\overline{\nu}_\tau p \to \tau^+ n; F_A, F_V, F_P(PCAC))}{\sigma(\overline{\nu}_\tau p \to \tau^+ n; F_A, F_V, F_P = 0)}. \tag{16}$$

for anti-neutrino quasi-elastic scattering, producing an additional $\sim 5\%$ reduction in the cross section for ν_τ resonance production.

As can be seen from Figures 3 and 4, the experimental uncertainties are quite large for these single pion states. The large number of different descriptions of these processes reflects a considerable theoretical uncertainty as well. The uncertainty in these cross sections could therefore reasonably be taken to be equal to the experimental uncertainties. Again, for the tau neutrino the situation is necessarily more uncertain since additional form factors, which are currently unmeasured, contribute.

4 Deep Inelastic Scattering

In the formalism of deep inelastic scattering, the neutrino scattering takes place off of the partons inside the nucleon. This process has been studied with high precision in the 20-200 of GeV energy range by a number of experiments (CCFRR, CHARM, CDHS) [18, 19, 20]. The following discussion follows Reference [21]. For such processes one again takes the most general form for the hadronic vertex summed over spin:

$$W_{\alpha\beta} = [W_1 M^2 \delta_{\alpha\beta} + W_2 p_\alpha p_\beta + W_3 \epsilon_{\alpha\beta\gamma\delta} p_\gamma Q_\delta/2 + W_4 Q_\alpha Q_\beta + W_5 (p_\alpha Q_\beta + p_\beta Q_\alpha)/2]. \tag{17}$$

In this expression W_j are the hadron form factors, p and p' are the initial and final momenta of the hadrons and $Q = (p' - p)$. The differential cross section can then be written:

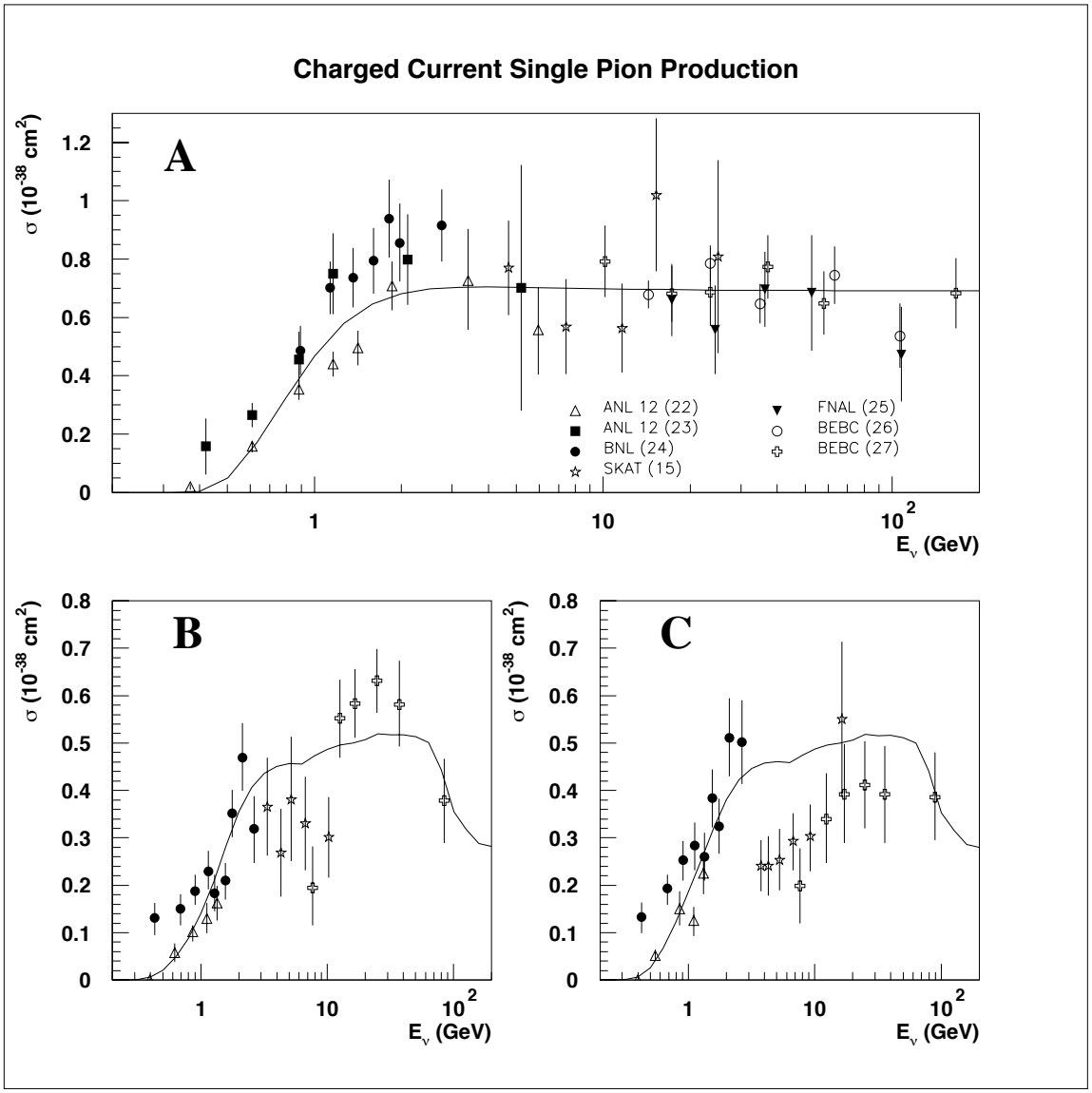

Figure 3: Charged Current Single Pion Production in the channels: A: $\nu_\mu p \to \mu^- \pi^+ p$ with W < 1.6 GeV. B: $\nu_\mu + n \to \mu^- n \pi^+$ with W < 2.0 GeV. C: $\nu_\mu + n \to \mu^- p \pi^0$ with W < 2.0 GeV. The solid line is the prediction of the Soudan 2 Monte Carlo.

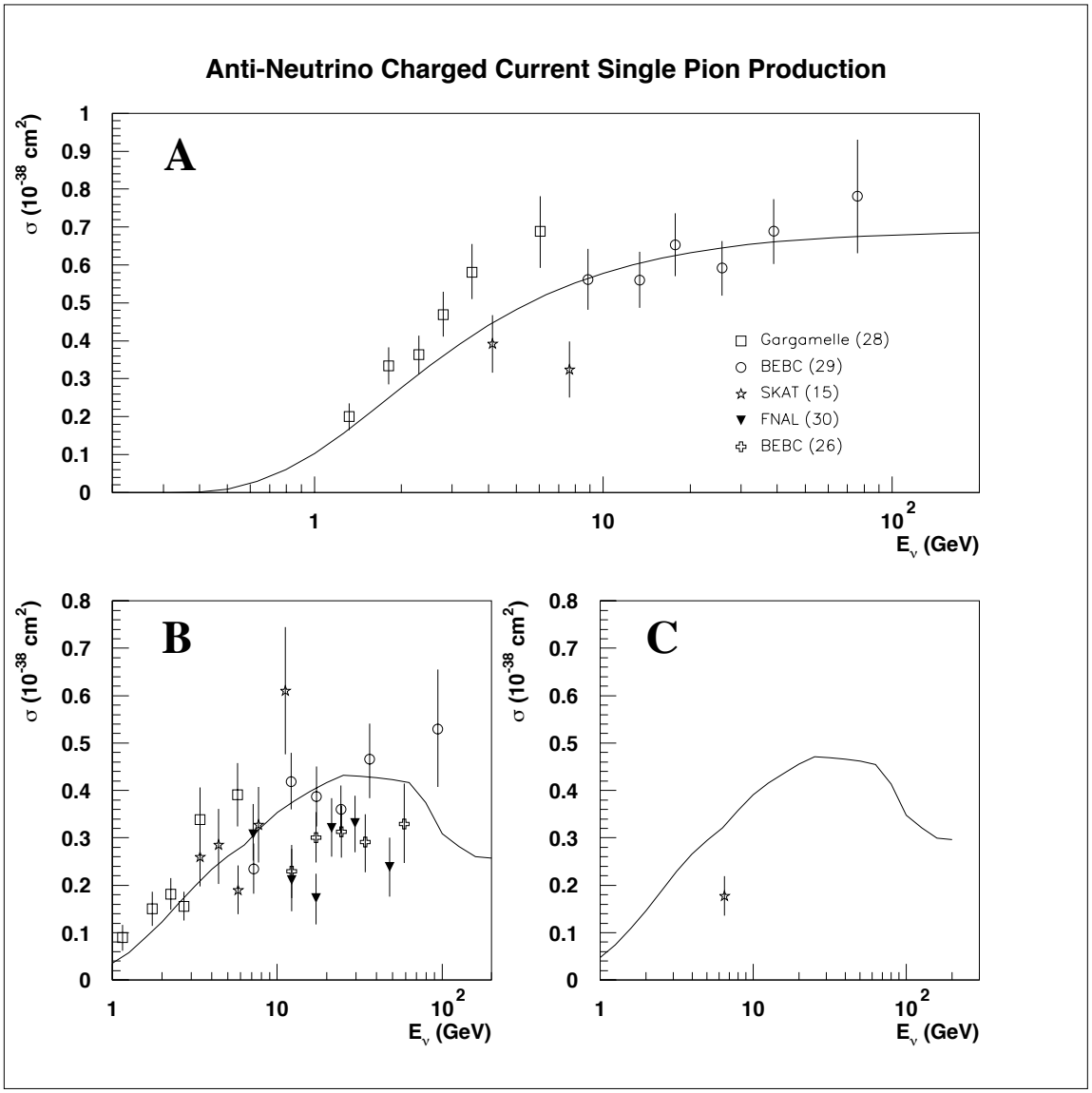

Figure 4: Charged Current Anti-Neutrino Single Pion Production in the channels: A: $\overline{\nu}_\mu n \rightarrow \mu^+ \pi^- n$ with W < 1.6 GeV. B: $\overline{\nu}_\mu p \rightarrow \mu^+ p \pi^-$ with W < 2.0 GeV. C: $\overline{\nu}_\mu + p \rightarrow \mu^+ n \pi^0$ with W < 2.0 GeV. The solid line is the prediction of the Soudan 2 Monte Carlo.

$$\frac{d^2\sigma}{dQ^2 d\nu} = \frac{G^2 E'}{2\pi E}\Big(\frac{M_W^2}{M_W^2+Q^2}\Big)^2\Big[\frac{W_2}{2}\Big(1+\frac{p_l}{E'}\cos\theta\Big)+W_1\Big(1-\frac{p_l}{E'}\cos\theta\Big) \tag{18}$$

$$\mp\frac{W_3}{2M}\Big(\frac{-m_l^2}{E'}+(E+E')\Big(1-\frac{p_l}{E'}\cos\theta\Big)\Big)+\frac{W_4 m_l^2}{2M^2}\Big(1-\frac{p_l}{E'}\cos\theta\Big)-\frac{W_5 m_l^2}{2ME'}\Big)\Big]$$

where G is the Fermi coupling constant, E, k and E', k' are the incoming neutrino and scattered lepton energies and 4-momenta, and θ is the scattering angle between the incoming neutrino and the outgoing lepton in the lab frame. Also, $\nu = E - E'$ and $-Q^2 = q^2 = (k-k')^2$. Alternatively, one can consider the process at the parton level. Writing the differential cross section for the neutrino-quark scattering, and summing over all quarks, the connection can be made between the form factors W1-W5 above and the parton distributions.

$$F_1 = MW_1; F_2 = \nu W_2 = \nu x W_5; F_3 = -\nu W_3; W_4 = 0 \tag{19}$$

where the variables x and y are related to q^2, ν by $x = q^2/(2M\nu), y = \nu/E$ and M is the nucleon mass. The differential cross section then becomes:

$$\frac{d\sigma}{dxdy} = \frac{G^2 ME}{\pi}\Big(\frac{M_W^2}{M_W^2+Q^2}\Big)^2\Big[F_2\Big(1-y-\frac{Mxy}{2E}\Big)+F_1 xy^2 \pm xF_3\Big(y-\frac{y^2}{2}\Big) \tag{20}$$

$$+\frac{m_l^2}{ME}\Big(-F_2\Big(\frac{M}{4E}+\frac{1}{2x}\Big)+\frac{F_1 y}{2}\mp\frac{F_3 y}{4}\Big)\Big].$$

The Callan-Gross relation $2xF_1 = F_2$ then simplifies the above expression further. It is then dependent on only two form factors, F_2 and F_3, which are given in terms of the parton distributions by

$$F_2 = \sum_i x(q_i + \overline{q}_i) \tag{21}$$

$$F_3 = \sum_i (q_i - \overline{q}_i). \tag{22}$$

We note that no additional assumptions were necessary to incorporate ν_τ interactions (through the inclusion of m_l^2 dependent terms) into the DIS formalism. The parton distributions are calculated in the usual way, with Q^2 behavior described by the Altarelli-Parisi equations. The situation is somewhat more complicated in the lower energy regime (10's of GeV), where perturbative QCD is of questionable validity. Most parton distributions have a range of validity which extends down to a cutoff Q^2 around 4 or 5 GeV^2. The Q^2 dependence of the partons distributions is then 'frozen' at this cutoff Q^2, i.e. for $Q^2 < Q_0^2$ the parton distributions are evaluated with $Q^2 = Q_0^2$. For a Q^2 cutoff of Q_0^2 and incident neutrinos of energy E, a fraction $f = \frac{Q_0^2}{2ME}(1 - \ln(\frac{Q_0^2}{2ME}))$ of phase space $x, y \in [0,1]$ has $Q^2 \leq Q_0^2$. For $E_\nu = 13$ Gev, a typical neutrino energy from the main injector wide band beam, and $Q_0^2 = 4\text{GeV}^2$, 44% of deep inelastic events have $Q^2 < Q_0^2$. One remedy is to use a set of

parton distributions which are valid to lower Q^2. For example, the GRV LO & HO sets employ a slightly different approach from other parton distributions in that they begin their QCD evolution at very low Q^2, a regime where the perturbative QCD evolution equations are of dubious validity. Nonetheless, these distributions are widely used, and claim to be valid over the range $.25\text{GeV}^2 \lesssim Q^2 \lesssim 10^6\text{GeV}^2$ [31]. At the present time, the Soudan 2 Monte Carlo uses the CTEQ 1M parton distributions, but we plan to switch over to the GRV LO set soon. The cross section for charged current muon neutrino deep inelastic scattering and the ratio of the tau neutrino to muon neutrino cross sections using the GRV-LO parton distributions are shown in figure 5. Since different choices for parton distributions can give significantly different predictions for the total cross section, the uncertainty in the charged current deep inelastic is equivalent to the experimental uncertainties. In this case, the tau neutrino cross sections are probably no more uncertain than the muon neutrino cross sections, since the cross sections for any lepton flavor are completely described once a set of parton distributions are chosen.

5 Forming σ_{tot}

There does not seem to be a consensus as to the best way to combine the quasi-elastic, resonance, and deep inelastic scattering cross sections at a fixed energy to form the total cross section. A number of different approaches have been suggested in the literature or used in practice. Recent preprints have discussed the effects that different prescriptions would have on calculations of rates of stopping and throughgoing neutrino-induced upward going muons [32]. A few different approaches include:

1. Including σ_{DIS} only. The kinematic region $M_N \leq W \leq M_N + M_\pi$ is non-physical for such processes, and by integrating $\frac{d\sigma}{dxdy}$ down to $W = M_N$ one includes quasi-elastic scattering and resonance production in a rough way.

2. $\sigma_{tot} = \sigma_{qel} + \sigma_{1\pi} + \sigma_{DIS}$ The single pion production cross section is calculated using one of the models described above, and the phase space integration for the calculation of DIS is limited to the region $W_0 < W$ to avoid double counting.

3. $\sigma_{tot} = \sigma_{qel} + \sum_j (\sigma^j_{Resonance} + f_j \sigma^j_{DIS})$

   Here the subscript j refers to the final state multiplicity. In this case the DIS cross section is written as a sum of exclusive cross sections for different final state multiplicities. Double counting is avoided on a multiplicity-by-multiplicity basis. The low multiplicity acceptance factors f_j are necessarily determined by comparing to data for each exclusive final state. In principle, f_j are energy dependent, in practice, however, this low multiplicity normalization is done at one fixed energy. For the Soudan Monte Carlo, this normalization is done at 20 GeV. At this energy, the amount removed from the deep inelastic cross section is equal to the resonance production cross sections in each of the multiplicity channels where both processes contribute [1]. Note here that

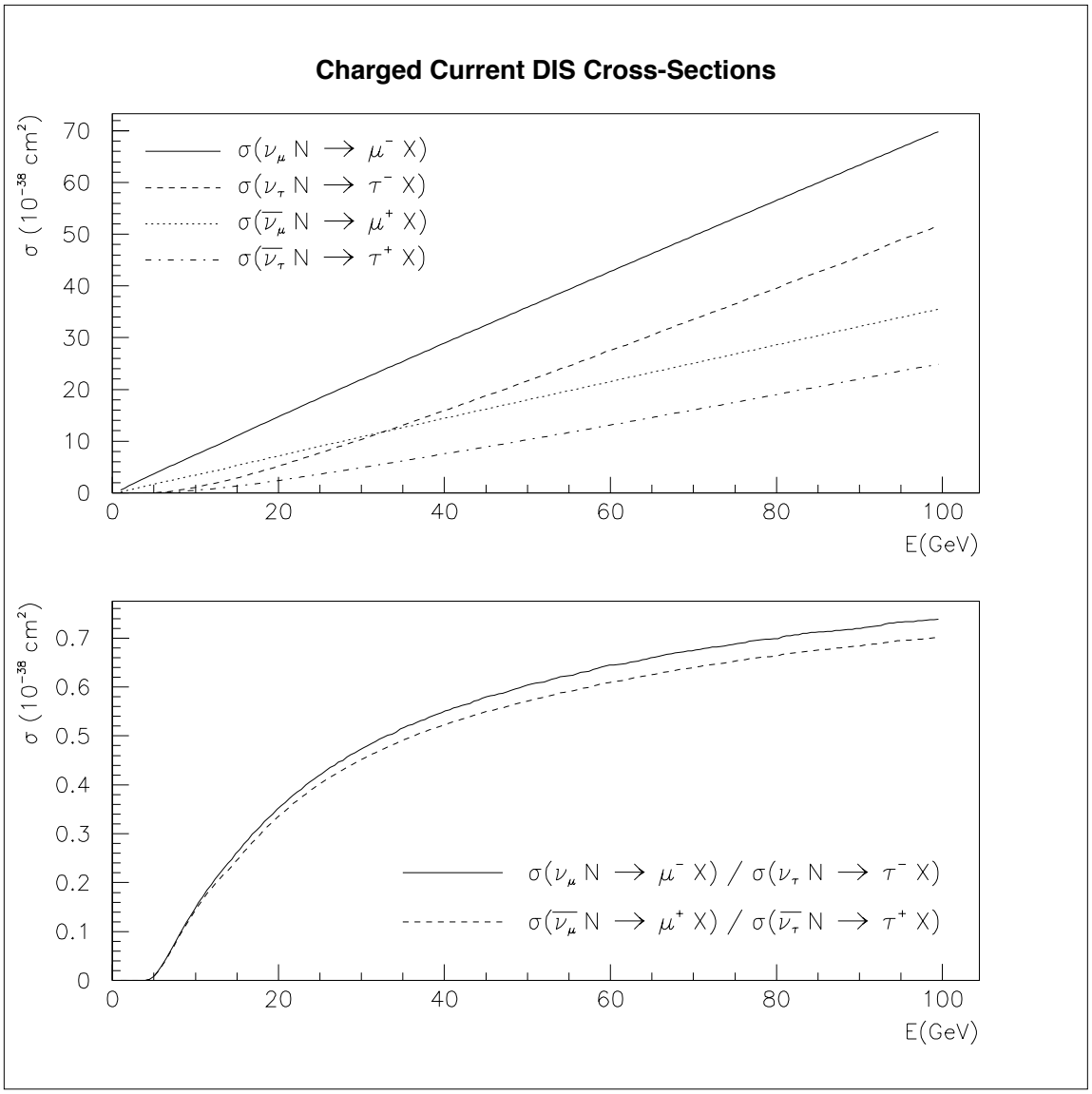

Figure 5: Charged Current Deep Inelastic Scattering Cross Sections

Interaction	f_2
$\nu + n \rightarrow l^- + (N + \pi)$	.240
$\overline{\nu} + p \rightarrow l^+ + (N + \pi)$	.240

Interaction	f_3
$\overline{\nu} + p \rightarrow l^+ + (N + 2\pi)$	.874
$\overline{\nu} + n \rightarrow l^+ + (N + 2\pi)$	.874
$\nu + p \rightarrow \nu + (N + 2\pi)$	.387
$\nu + n \rightarrow \nu + (N + 2\pi)$	.387
$\overline{\nu} + p \rightarrow \overline{\nu} + (N + 2\pi)$	.133
$\overline{\nu} + n \rightarrow \overline{\nu} + (N + 2\pi)$	.133

Table 1: Deep inelastic scattering low multiplicity inclusion factors f_j

this prescription is necessarily dependent on the hadronization scheme for DIS events, as different algorithms can produce different final state multiplicities σ^j_{DIS} for the same total DIS cross section.

In principle, comparing to differential distributions for low multiplicity final states (1 and 2 π) yields additional information about the validity of the above approaches, however data is sparse in such states and conclusions are thus hard to make. The Soudan 2 simulation employs method 3 above, with a hadronization scheme which is based on KNO scaling [1]. The averaged charged particle multiplicity in neutrino interactions has been observed to rise linearly with W^2 [33]. Fits can thus be done to multiplicity distributions of the form

$$< n >= a + b \ln W^2. \tag{23}$$

KNO scaling asserts that the scaled multiplicity distribution $< n > P(n, W)$ plotted as a function of $n/ < n >$ should be independent of W, and this is indeed seen to hold in hadronic final states produced in neutrino interactions [34, 35]. Plots B and C of Figures 3 and 4 include the DIS contribution to these final states. Note that plot A in each figure corresponds to an isospin 3/2 state, which can be fit completely in terms of resonance production.

Of course any method we choose must agree with the data. All three of the above methods must obviously agree in their predictions for σ_{tot}. Data exist for many low multiplicity exclusive final states, which must be used to determine the W-cut in method 2 and the DIS low multiplicity inclusion factors f_j in method 3. The factors f_j as used in the Soudan 2 Monte Carlo are given in Table 3.

The predictions of the Soudan Monte Carlo for σ_{tot} are compared to the available data in Figure 6. The expected event rates for atmospheric and long baseline neutrinos under a number of different oscillation scenarios are given in Tables 2 and 3.

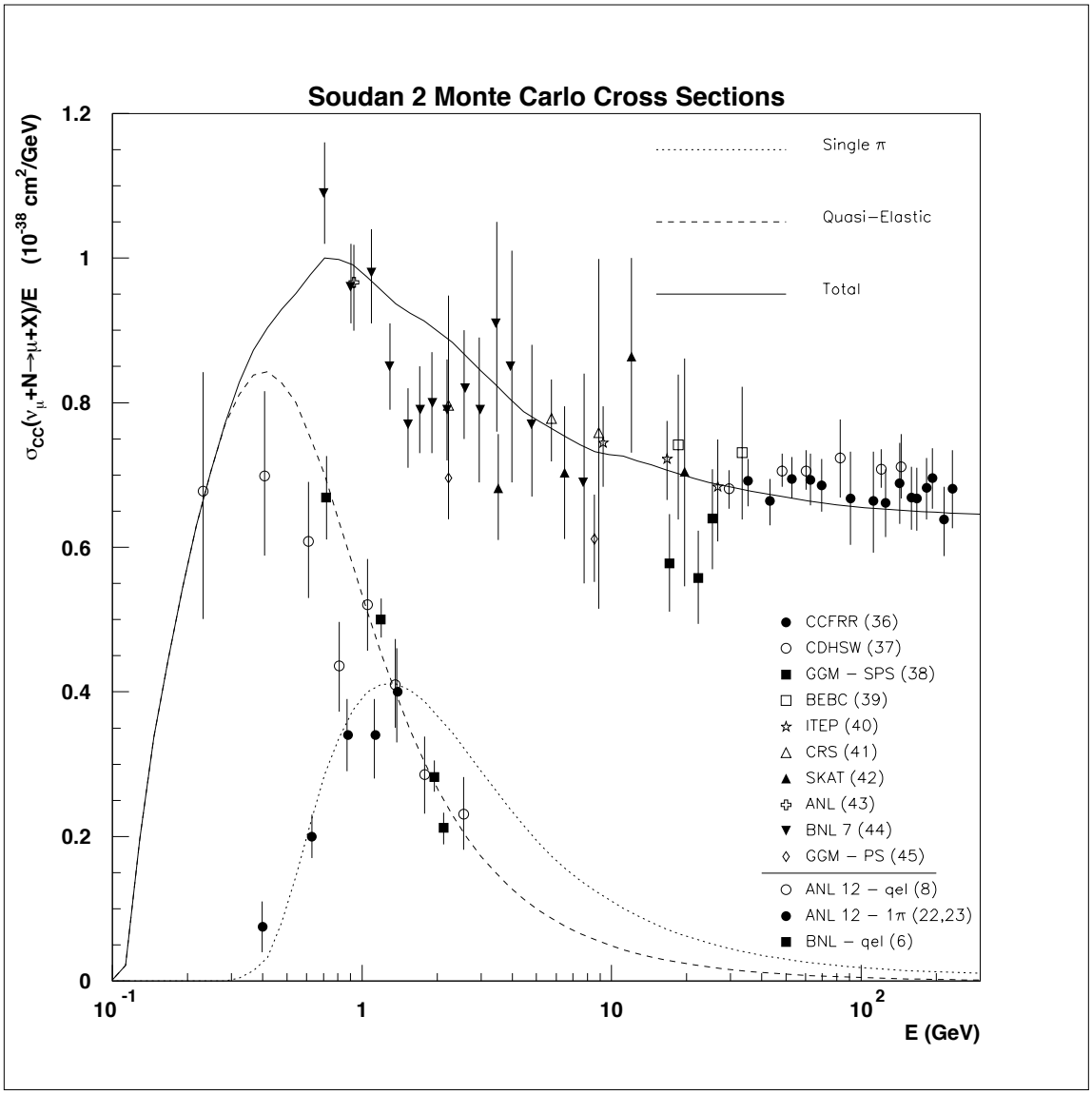

Figure 6: Cross Sections versus energy for an isoscalar target. Data compiled by [46]

A. No Oscillations

	QEL		Inelastic	
	NC	CC	NC	CC
ν_e	27.1	65.7	6.8	26.3
$\overline{\nu}_e$	12.0	17.1	2.3	6.6
ν_μ	51.5	99.3	14.0	47.1
$\overline{\nu}_\mu$	27.0	30.0	5.5	13.3
ν_τ	.0	.0	.0	.0
$\overline{\nu}_\tau$	.0	.0	.0	.0

B. Kamiokande Point: $\sin^2(2\theta) = .69, \Delta m^2 = .01 eV^2$

	QEL		Inelastic	
	NC	CC	NC	CC
ν_e	27.1	65.7	6.8	26.3
$\overline{\nu}_e$	12.0	17.1	2.3	6.6
ν_μ	33.6	64.8	10.4	35.1
$\overline{\nu}_\mu$	17.7	19.8	4.1	10.0
ν_τ	18.0	.1	3.6	.3
$\overline{\nu}_\tau$	9.3	.1	1.4	.1

C. 3-Flavor Maximal Mixing [48]: $\sin^2(2\theta) \approx 2/9, \Delta m^2 = .007 eV^2$

	QEL		Inelastic	
	NC	CC	NC	CC
ν_e	26.4	64.0	6.8	26.0
$\overline{\nu}_e$	12.6	17.9	2.3	7.0
ν_μ	34.6	67.8	10.8	36.5
$\overline{\nu}_\mu$	17.7	20.1	4.3	10.3
ν_τ	17.6	.1	3.3	.3
$\overline{\nu}_\tau$	8.7	.0	1.3	.1

Table 2: Atmospheric neutrino events/kiloton-year in the Soudan 2 detector. Fluxes are from [47], the cross sections used are those described in this document.

A. No Oscillations

	QEL		Inelastic	
	NC	CC	NC	CC
ν_e	.3	.6	5.0	16.9
$\overline{\nu}_e$	.0	.1	.6	1.7
ν_μ	45.9	117.3	623.6	2071.9
$\overline{\nu}_\mu$	.7	1.4	4.6	13.2
ν_τ	.0	.0	.0	.0
$\overline{\nu}_\tau$	.0	.0	.0	.0

B. Kamiokande Point: $\sin^2(2\theta) = .69, \Delta m^2 = .01 eV^2$

	QEL		Inelastic	
	NC	CC	NC	CC
ν_e	.2	.6	5.0	16.8
$\overline{\nu}_e$	0.	.1	.6	1.7
ν_μ	29.7	75.8	463.3	1538.3
$\overline{\nu}_\mu$	.4	.9	3.3	9.5
ν_τ	16.2	25.1	160.3	103.5
$\overline{\nu}_\tau$	.2	.3	1.3	.6

C. 3-Flavor Maximal Mixing [48]: $\sin^2(2\theta) \approx 2/9, \Delta m^2 = .007 eV^2$

	QEL		Inelastic	
	NC	CC	NC	CC
ν_e	7.6	19.6	68.6	231.6
$\overline{\nu}_e$	.2	.3	1.0	3.0
ν_μ	31.1	79.3	495.7	1644.3
$\overline{\nu}_\mu$	.5	1.0	3.6	10.3
ν_τ	7.5	10.1	64.4	37.0
$\overline{\nu}_\tau$	.1	.1	.6	.2

Table 3: Long baseline neutrino event rates at Soudan. The tables are neutrino events/standard-kiloton-year on an iron target. Fluxes are from [49], using the cross sections described in this document.

Acknowledgements

The authors would like to thank S. Mrenna for numerous helpful discussions.

References

[1] Giles Barr, Ph. D. Thesis, Oxford University, (1987).

[2] C. H. Clewellyn Smith. Phys. Rep., **3C**, 261 (1971).

[3] R. P. Feynman and M. Gell-Mann, Phys. Rev. **109**, 193 (1958).

[4] M. Gell-Mann and M. Levy, Nuovo Cimento, **16**, 705 (1960).

[5] C. W. Kim and A. Pevsner, Neutrinos in Physics and Astrophysics, (Harwood Academic Publishers, Langhorn, PA), 69 (1993).

[6] N. J. Baker *et al.*, Phys. Rev. **D23**, 2499 (1981).

[7] F. Boehm and P. Vogel, Physics of Massive Neutrinos. Cambridge University Press, Cambridge, 46 (1992).

[8] W. A. Mann *et al.*, Phys. Rev. Lett. **31**, 844 (1973); S. J. Barish *et al.*, Phys. Rev. **D16**, 3103 (1977).

[9] T. Kitagaki *et al.*, Phys. Rev. **D28**, 436 (1983).

[10] W. M. MacDonald, E. T. Dressler, and J. S. O'Connell, Phys. Rev. **C19**, 455 (1979).

[11] M. R. Adams *et al.*, Z. Phys. C. **67**, 403 (1995).

[12] R. P. Feynman, M. Kislinger, and F. Ravndal, Phys Rev. **D3**, 2706 (1971).

[13] Rein and Seghal, Ann. Physics (NY), **133**, 79 (1981).

[14] P. Allen *et al.*, Nuclear Physics **B176**, 269 (1980).

[15] H. J. Grabosch, *et al.*, Z. Phys **C41**, 527 (1989).

[16] S. L. Adler, Annals of Physics, **50**, 189 (1968).

[17] G. L. Fogli and G. Nardulli, Nuclear Physics B, **160**, 116 (1979).

[18] R. Blair *et al.*, Physics Review Letters **51**, 343 (1983).

[19] M. Jonker *et al.*, Physics Letters **B99**, 265 (1081). Physics Letters **B100**, 520(E) (1981).

[20] P. Berge *et al.*, Z. Physics **C38**, 403 (1988).

[21] B. P. Roe, NUMI-29, 1994.

[22] G. M. Radecky *et al.*, Phys. Rev. **D17**, 1161 (1982).

[23] J. Campbell *et al.*, Phys. Rev. Lett. **30**, 335 (1973).

[24] T. Kitagaki *et al.*, Phys. Rev. **D34**, 2554 (1986).

[25] J. Bell *et al.*, Phys Rev. Lett. **41**, 1008 (1978).

[26] P. Allen *et al.*, Nucl. Phys. **B264**, 221 (1986).

[27] S. Barlag, Ph. D. Thesis, Amsterdam, (1984).

[28] T. Bolognese *et al.*, Phys. Lett. **B81**, 393 (1979).

[29] P. Allasia *et al.*, Z. Phys. **C20**, 95 (1983).

[30] S. J. Barish *et al.*, Phys. Lett. **B91**, 161 (1980).

[31] Glück, Reya, Vogt, Z. Physics **C53**, 127 (1992).

[32] P. Lipari *et al.*, ROMA Preprint n. 1072, (1994).

[33] P. Allen *et al.*, Nuclear Physics **B181**, 385 (1981).

[34] Z. Koba, H. B. Nielsen, P. Olesen, Nuclear Physics **B40**, 317 (1972).

[35] N. Schmitz, Proc. Intl. Symp. on Lepton and Photon Interactions at High Energies, Bonn, 527 (1981).

[36] D. B. MacFarlane *et al.*, Z. Phys. **C26**, 1 (1984).

[37] P. Berge *et al.*, Z. Phys. **C35**, 443 (1987).

[38] J. Morfin *et al.*, Phys. Lett. **104B**, 235 (1981).

[39] D. C. Colley *et al.*, Z. Phys. **C2**, 187 (1979).

[40] A. S. Vovenko *et al.*, Sov. Jour. Nucl. Phys. **30**, 527 (1979).

[41] D. S. Baranov *et al.*, Phys. Lett. **81B**, 255 (1979).

[42] C. Baltay *et al.*, Phys. Rev. Lett. **44**, 916 (1980).

[43] S. J. Barish *et al.*, Phys. Rev. **D19**, 2521 (1979).

[44] N. J. Baker *et al.*, Phys. Rev. **D25**, 617 (1982).

[45] S. Ciampolillo *et al.*, Phys. Lett. **84B**, 281 (1979).

[46] Particle Data Group, Phys. Rev. D, **D50**, (1992).

[47] T. Gaisser, T. Stanev, G. Barr, Phys. Rev. **D38**, 85 (1988); and G. Barr, T. Gaisser, T. Stanev, Phys. Rev. **D39**, 3532 (1989).

[48] P.F. Harrison, D.H. Perkins, and W.G. Scott, Phys. Lett. **B349**, 137 (1995).

[49] Maury Goodman, NuMI-L-49, 1994.